13th International Symposium on Particle Image Velocimetry – ISPIV 2019
Munich, Germany, July 22-24, 2019

Influence of time interval between two snapshots on the measurement accuracy of stereoscopic PIV

Qigang Chen[1]*, Qiang Zhong[2]

[1] Beijing Jiaotong University, School of Civil Engineering, Beijing, China

[2] China Agricultural University, College of Water Resources & Civil Engineering, Beijing, China

*chenqg@bjtu.edu.cn

Abstract

The present study investigates the influence of time interval between two particle images in each pair on the measurement accuracy of stereo-PIV with experimental data sets of a laminar flow and a turbulent open channel flow with Re_τ=1040. The results indicate that the one-quarter rule should be strictly followed when performing stereo-PIV measurement. Moreover, two additional practical suggestions are proposed for carrying out stereo-PIV measurements. Firstly, for flows with negligible velocity gradient, a larger time interval is useful for improving the measurement accuracy. Secondly, for flows with large velocity gradient, displacement gradient in the interrogation window dominates the measurement accuracy, and a smaller time interval is necessary for a better measurement accuracy. A direct deduction from these two suggestions is that the near-wall region and outer-region of wall turbulences should be measurement with different stereo-PIV parameters.

1 Introduction

Stereoscopic particle image velocimetry (Stereo-PIV) is a non-intrusive measurement technique capable of measuring the three-dimensional (3D) velocity fields in a plane (Arroyo and Greated, 1991). It adopts two cameras to record simultaneously the images of particles in the flow illuminated by a laser sheet with different viewing angle. The particle images recorded by each camera are used to calculate two dimensional (2D) velocity fields with PIV algorithm. The 3D velocity fields are then reconstructed based on the differences between a pair of two 2D velocity fields (Prasad and Adrian, 1993). The principle of SPIV implies its measurement accuracy is determined by the 2D velocity fields and the reconstruction process.

The error sources in the reconstruction process of stereo-PIV include the imaging configuration, the calibration model, and the reconstruction algorithm. Compare with the PIV measurement, the in-plane velocity of stereo-PIV is more accurate due to the elimination of perspective error. Therefore, researches on the measurement accuracy of stereo-PIV mainly focus on the error of the out-of-plane velocity. Plenty of theoretical and experimental results have shown the out-of-plane error is larger than the in-plane one, and the error ratios are determined by the imaging configuration as follows (Lawson and Wu, 1997a, 1997b).

$$\frac{\sigma_{\Delta z}}{\sigma_{\Delta x}} = \frac{1}{\tan\theta} \qquad (1)$$

Where, $\sigma_{\Delta z}$ is the out-of-plane error, $\sigma_{\Delta x}$ is the in-plane error, and θ is the viewing angle of the symmetrically placed cameras. Equation (1) indicate that the accuracy of the out-of-plane velocity increases with the viewing angle of the camera, and all velocity components have the same accuracy when the viewing angle is 45°. The influences of calibration model and reconstruction method on the measurement accuracy of stereo-PIV were evaluated during the third international PIV challenge. Results show no extra errors were introduced by the reconstruction process when standard imaging configuration was adopted (Stanislas et al. 2008). Recently, results of the fourth international PIV challenge further prove the choices of calibration models and reconstruction methods have relatively little effect on the quality of the out of plane velocity (Kähler et al. 2016). Therefore, under the condition that the stereo-PIV system was ideally configured, increasing the accuracy of the 2D velocity fields becomes crucial for reducing the measurement error of stereo-PIV technique. Accordingly, the influences of time interval or time delay between two particle images (snapshots) in a pair on the measurement accuracy of stereo-PIV relate tightly with the influences of time interval on the measurement accuracy of planer PIV technique.

The influences of time interval on the measurement accuracy of planer PIV technique have been extensively studied by Keane and Adrian (1990, 1991, and 1992). Their results indicated the time interval should be short enough to ensure highly detectable correlation between particle images in two successive interrogation windows. Accordingly, several well-known designing rules were proposed to limit the loss of particles due to in-plane motion, out-of-plane motion, and the spatial gradient of particle displacement within the interrogation window. Among these rules, the one-quarter rule has been widely followed even after the introduction of advance image interrogation algorithms such as the image or window deformation techniques.

However, even under the condition that the one-quarter rule is satisfied, the time interval can influence the measurement accuracy of planer PIV. For example, if a PIV system records particle images with diameters larger than 2.0 pixels, the error in the calculated displacements can be expressed as $\sigma_{\Delta x}=c_\tau d_\tau$ (Adrian 1997). Here, d_τ is the size of a pixel; c_τ is a measure for the ability of the interrogation algorithm to accurately determine the particle image displacement, and it is typically of the order of 0.05–0.2 (Westerweel et al. 2013). If the error of the time interval is negligible, the measurement error of the velocity can be expressed as:

$$\sigma_u = \frac{\sigma_{\Delta x}}{\Delta t} = \frac{c_\tau d_\tau}{\Delta t} \qquad (2)$$

Equation (2) shows clearly the measurement error of velocity reduces with the increasing of time interval. The experimental study carried out by Poelma et al. (2006) in grid-generated turbulence also indicated the measurement accuracy of PIV improves with the increasing of time interval within the range where the one-quarter rule is satisfied.

Obviously, most existing researches have ignored the influence of time interval on the displacement gradient within the interrogation window and therefore on the measurement accuracy of PIV. Meanwhile, the influence of time interval on the measurement accuracy of stereo-PIV has not been directly studied. Therefore, the present study uses two typical experimental data sets to investigate the influence of time interval on the measurement accuracy of stereo-PIV.

2 Data Sets and Methodology

2.1 Laminar Flow Data Set

The laminar flow data set is the case E data of the fourth international PIV challenge. The experiment generated the data was conducted by professor Rod La Foy's group at Virginia Tech. The flow field contains an impulsively started axisymmetric laminar vortex ring. Particles in the flow field were illuminated by a laser sheet and were recorded by five high-speed cameras with different viewing angles at 1000 Hz. The particle images acquired at the same time were processed as a three-dimensional tomographic PIV measurement to obtain 3D velocity fields which were used as

references for evaluating the accuracy of the stereo-PIV measurement. Details on the experiment and data set can be found in Kähler et al. (2016). Images recorded by two of the five cameras were used for evaluating the performance of stereo-PIV technique.

The present study used the 100 pairs of images provided by the committee to evaluate the influence of time interval on the measurement accuracy of stereo-PIV. Due to its time-resolved property, the time interval δt_u between every two successive particle images is 0.001 s. In order to change the time interval between particle images in each pair, two images separated by different number of images were resampled to form an image pair. The image pairs recorded simultaneously by the two cameras were processed with stereo-PIV algorithm to obtain the measured 3D velocity field. For example, when images n and $n+k$ recorded by each camera were processed with stereo-PIV algorithm to calculate the 3D flow field, the time interval between two snapshots is $\delta t = k\delta t_u$. Meanwhile, if we define the time for recording the first image to be t=0, the measured velocity field is at the time $t = (n\text{-}1+k/2)\ \delta t_u$.

2.2 Wall Turbulence Data Set

The wall turbulence data set was obtained through a measurement of a uniform open channel turbulence. The experiment was conducted in a recirculating tilting water flume located at Tsinghua University. The flume is 20 m long and 0.3 m wide, with a glass bed and glass side walls. Details on the experimental facility can be found in Chen et al. (2014). The bed slope of the flume was 0.002, and the flow depth is 4.0 cm. The test section is 12m downstream of the entrance. Velocity fields in the streamwise–wall-normal plane located midway between the side walls were measured with a time-resolved Stereo-PIV system. The water flow was seeded with hollow grass particles with a mean diameter of 10 μm, and a specific gravity of 1.06. These particles were illuminated by a 1.5mm thick laser sheet generated by a Nd:YLF laser. The pulse energy of the laser sheet is 10mJ when operated at the frequency of 1000 Hz. Particle images were recorded simultaneously by two high speed cameras having a frame rate of 730 at the full resolution of 2336×1920 pixels. Each camera were connected to a Nikon AF 50mm f/1.8D lens with a Scheimpflug adaptor. These two cameras were fixed nearly symmetrically at the upstream and downstream sides of the measurement section with a valid view angel of about 24°. The cameras and laser were synchronized by a Quantum® QC9524 pulse generator with a time accuracy of ±1 ns.

The imaging resolution of each camera is about 16 pixel/mm. The common field of view of the two cameras is about 11×4.0cm. Particle images were recorded successively at a frequency of 1000Hz. The measurement lasts about 80s to sample more than 800 independent velocity fields. In order to investigate the influence of time interval between two particle images on the measurement accuracy, the images were processed with the same method documented in section 2.1.

2.3 Methodology

The 3D velocity fields were obtained by interrogating the particle images with a home-made stereoscopic software. The images were preprocessed with a contrast-stretching transformation and a Gaussian filter. The processed images recorded by each camera were then interrogated with classic cross correlation method using multipass, multigrid, and image deformation algorithm to obtain the 2D velocity fields. For the laminar flow data set, the particle images were processed with a multi-frame pyramid correlation method proposed by Sciacchitano et al. (2012) as well. The interrogation window for the laminar flow were 32×32 and 28×28 with an overlap ration of 50% for camera 1 and camera 2, respectively. The interrogation window for the turbulent open channel flow were 24×24 and 20×20 with an overlap ration of 50% for camera 1 and camera 2, respectively.

The 2D velocity fields measured at the same time were adopted to reconstruct the 3D velocity field with the Soloff method (Soloff et al. 1997). The mapping function is a polynomial with cubic dependence in *x* and *y* and quadratic dependence in *z*. Coefficients of the function were determined by placing calibration targets in the measurement region and performing non-linear least-square regressions. Meanwhile, the mapping function was refined by a self-calibration method (Wieneke, 2005). The reconstructed 3D velocity vectors were distributed on a 0.5×0.5 mm grids.

According to the flow regime, the image interrogation method, and the time-interval between two particle images, a total of 11 cases were analyzed in the present study. Details about each case were listed in Table 1. Here, the initial letters L and T in the case name indicate laminar flow and turbulence, respectively. The following letters CC and PC denotes classic two-frame cross-correlation algorithm and multi-frame pyramid correlation algorithm, respectively. The velocity component in the *x*, *y*, and *z* direction are denoted by *U*, *V*, and *W*, respectively. For the laminar flow, the z-axis is the perpendicular to the measurement plane. For the turbulent open channel flow. The *x*-axis is oriented along the main flow, the *y*-axis is normal to the bed and pointing toward water surface, and the transverse *z*-axis is normal to the flume side wall.

For the laminar flow cases, the accuracy of SPIV measurements were evaluated by comparing the measured 3D velocity fields with the reference 3D velocity fields. On the other hand, the measurement accuracy of the turbulent open channel flow were evaluated by analyzing the vertical distributions of mean velocities, turbulent intensities, and Reynolds shear stresses.

Table I: Flow regime, image interrogation method, and time interval for each case

Case	δt (s)	Case	δt (s)	Case	δt (s)
CC1	0.001	LPC1	0.001	TCC1	0.001
LCC2	0.002	LPC2	0.002	TCC2	0.002
LCC3	0.003	LPC3	0.003	TCC3	0.003
LCC4	0.004	LPC4	0.005	TCC4	0.004
LCC5	0.005				
LCC6	0.006				
LCC7	0.007				

3 Results

3.1 Laminar Flow

For the laminar flow, the measurement error of each velocity vector at a specified position and time were calculated as follows:

$$\begin{aligned} \Delta U &= \left| U_m - U_r \right| \\ \Delta V &= \left| V_m - V_r \right| \\ \Delta W &= \left| W_m - W_r \right| \end{aligned} \tag{1}$$

Here, subscripts “m” and “r” indicate measured value and reference value, respectively. The mean value and standard deviation of the error of each velocity component were calculated and presented in Figure 1. For results obtained with different interrogation methods, the measurement errors

decrease gradually with the increasing of time interval under the condition that the one quarter rule is satisfied. Then, the errors tend to increase slightly if the time interval increases further. In general, cases LCC6 and LPC2 show the best performances for the two interrogation methods, respectively. Compare with the results of classic cross correlation method, the velocity fields processed with multi-frame pyramid correlation method contain smaller errors. Among different components of the velocity vectors, the errors in the in-plane velocities are comparable and are smaller than that of the out-of-plane velocity.

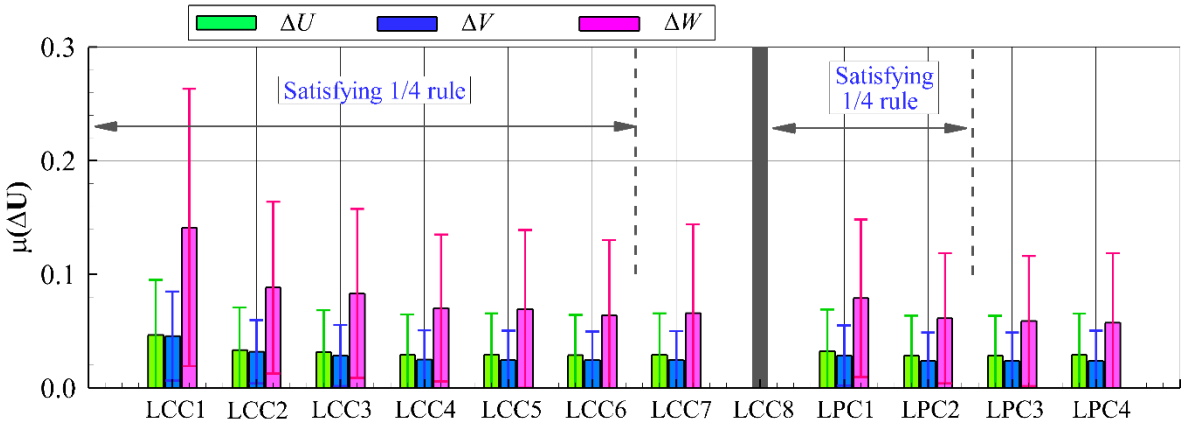

Figure 1: Mean values (bars) and standard deviations (whiskers) of measurement error of each velocity component.

Figure 2 presents the error ratios between the in-plane velocities and the out-of-plane velocity. The dashed horizontal line represents the theoretically expected ratios based upon the geometric configuration of the cameras. The results for cases LCC2, LCC3, LCC4, LCC5 and LPC1 indicate that the present self-calibration algorithm work quite well as the measured error ratio agreeing well with the theoretical value. Among different cases, the error ratios decrease slightly with the increasing of the time interval. In general, the accuracy of the out-of-plane velocity is mainly a function of the accuracy of the in-plane velocity

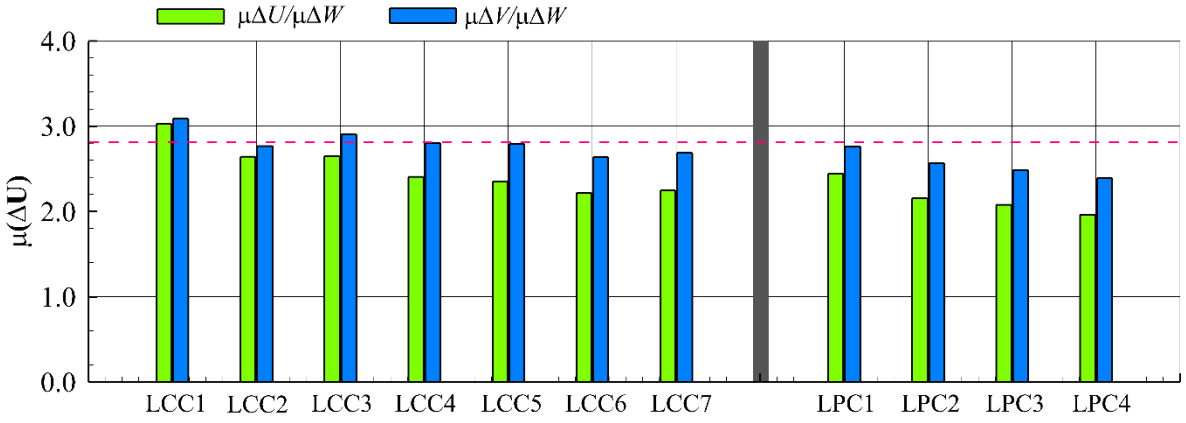

Figure 2: Error ratios between the in-plane and out-of-plane velocities for different cases

Figure 3 presents the distributions of the total error of the measured velocity vectors in each case. The error distributions qualitatively follow a log-normal behavior. In figure 3(a), case LCC6 shows the narrowest spread. In figure 3(b), distributions except for that of case LPC1 are nearly overlap

with each other. The error distributions also indicate that within the range when the one quarter rule is satisfied, the measurement accuracy improves with the increasing of the time interval.

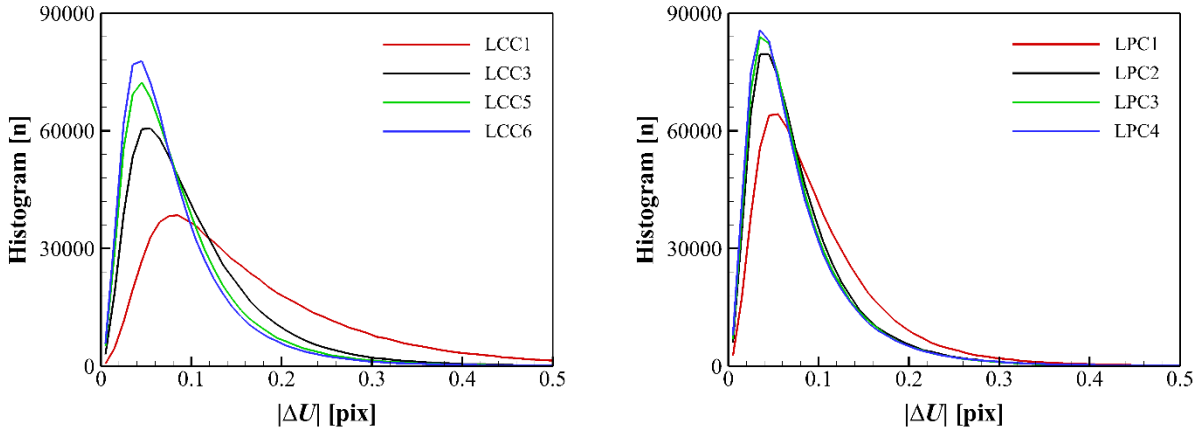

(a) cross correlation method (b) pyramid correlation method

Figure 3: Distributions of the total error of velocity vectors calculated with different method

Figure 4 presents a typical instantaneous velocity field. The measured velocity field for case LPC2 in figure 4(a) is quite similar with the reference velocity field in figure 4(b). The in-plane velocity components reveal the existence of a pair of counter-rotating vortices. The out-of-plane velocity component indicates the fluid flow in contrast directions on the left and right sides of the vortices.

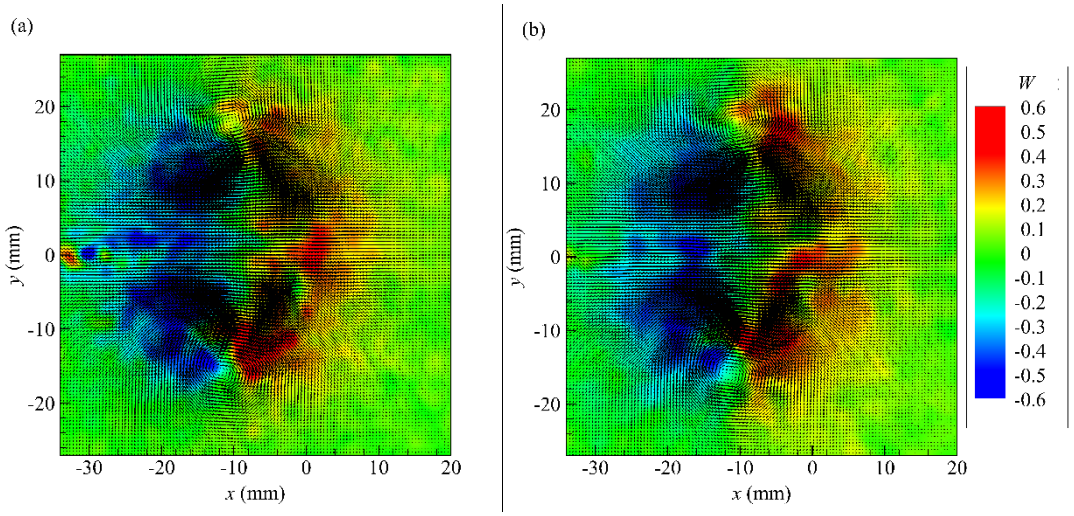

Figure 4: A typical (a) calculated instantaneous velocity field for case LPC2 and its corresponding (b) reference velocity field. Vectors and color contours indicate in-plane and out-of-plane velocity components, respectively.

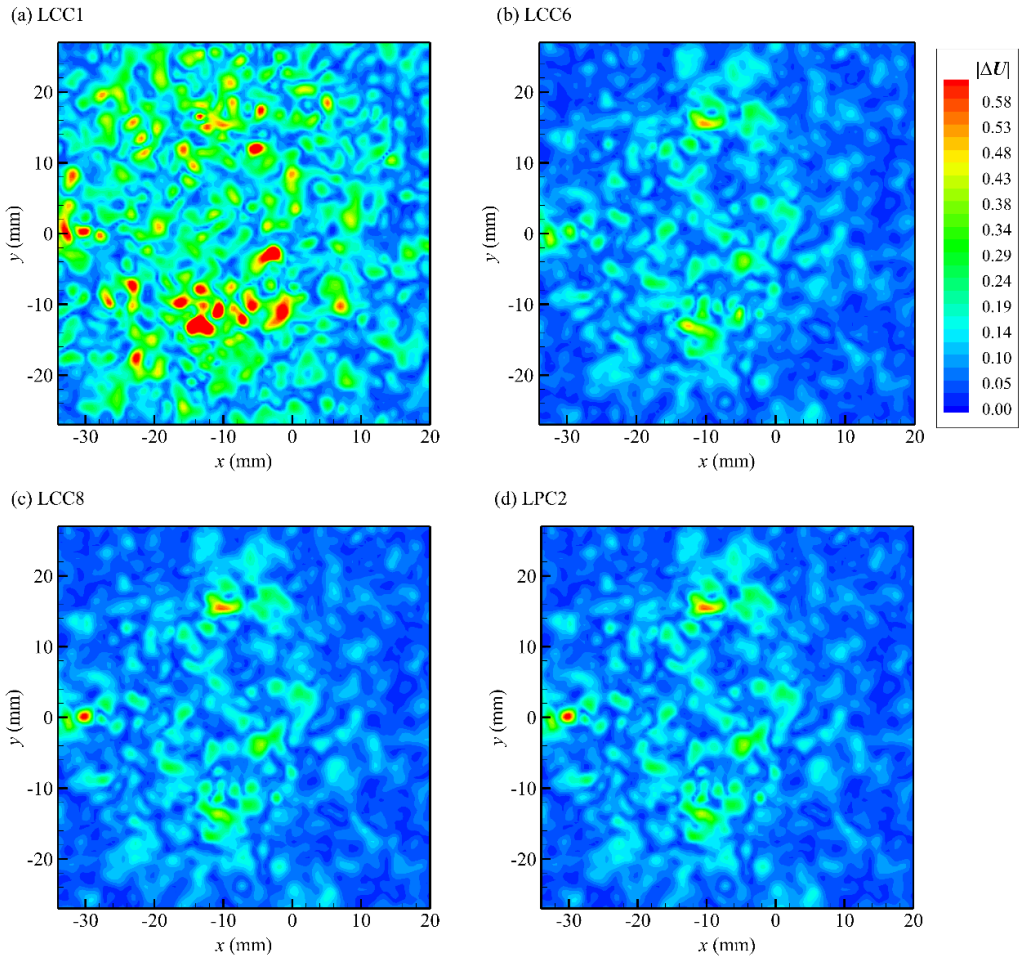

Figure 5: Distributions of the total error in the velocity field shown in figure 4 for different cases.

Figure 5 presents distributions of the total measurement error for difference cases in the instantaneous velocity field shown in figure 4. For case LCC1 which shows the lowest performance, the total error in figure 5(a) distributes uniformly in the whole flow field. However, for cases show much better performance in figures 5(b), 5(c), and 5(d), the measurement errors appears mainly within the vortex core region where high shear significantly impacts the accuracy of both the in-plane and out-of-plane velocity estimations. A notable feature in figures 5 is that relatively large errors were observed around the point x=-30 and y=0 for all cases. The velocity gradient distributions (not shown) indicate that the component $\partial V/\partial y$ show maximum here. Therefore, it seems that large velocity gradient can result in elevated measurement error in the stereo-PIV measurement. Moreover, the error induced by velocity gradient is expected to increase with the increasing of time interval.

3.2 Turbulent Open Channel Flow

After obtaining all the measured 3D velocity fields for each case, the vertical distributions of the mean velocities, turbulent intensities, and Reynolds shear stress were calculated. The results were presented in figures 6-8. In order to qualitatively evaluate the measurement accuracy, the results of direct numerical simulation (DNS) of a channel flow with Re_τ=950 were included for comparison.

Figure 6 presents the vertical distributions of the mean velocities. In figure 6(a), the streamwise mean velocity for different cases overlap with each other and that of the DNS very well in the region y+ > 100. However, the measured profiles in the near-wall region deviate quickly from the DNS profile with the increasing of the time interval. In figure 6(b), the vertical mean velocity for all cases is zero within the whole water depth. In figure 6(c), the influence of the time interval on the spanwise mean velocity is the same as that of the streamwise mean velocity. The results indicate that changing the time interval have negligible influence, if only, on the measured mean velocity in regions where the velocity gradients are quite small. However, increasing the time interval results in increasing measurement errors in both in-plane and out-of-plane velocity components in high shear region.

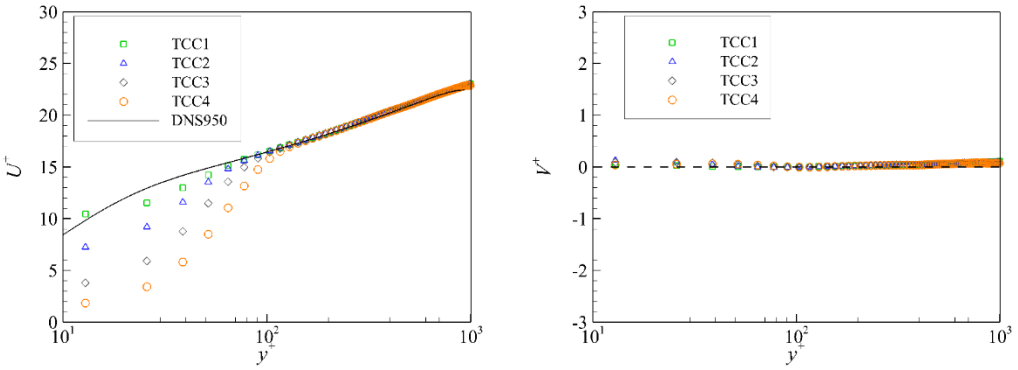

(a) streamwise mean velocity (b) vertical mean velocity

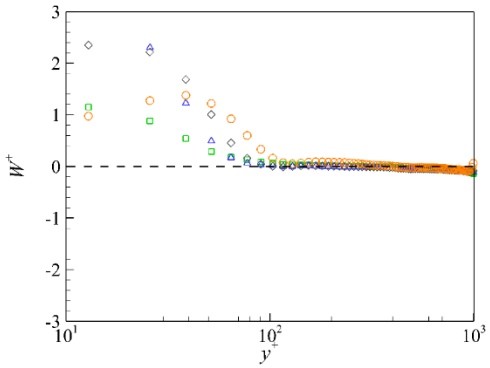

(c) spanwise mean velocity

Figure 6: Profiles of the mean velocities of turbulent open channel flow for different cases

Figure 7 presents the vertical profiles of streamwise, vertical, and spanwise turbulent intensities for all cases. The turbulent intensities of the DNS channel flow were plotted for facilitating interpretation. However, one should note that the vertical distributions of turbulent intensities depends both on the outer boundary condition and the Reynolds number (Hultmark et al. 2010; Ghosh et al. 2010). Therefore, the results of the turbulent open channel flow are not expected to be the same as those of the turbulent channel flow even. Nevertheless, the distributions of the turbulent intensities in the near-wall region of different flows should be qualitatively similar. The results suggest that in the region of y^+ >100, the measurement accuracies of the turbulent intensities

are not influenced by the time interval. In the near wall region, the vertical turbulent intensity exhibit negligible variance with the time interval. However, the streamwise and spanwise turbulent intensities are significantly influenced by the time interval, and the measurement accuracy reduces with the increasing of the time interval. The increasing of $\partial U/\partial y$ within the interrogation window is the main cause of measurement errors.

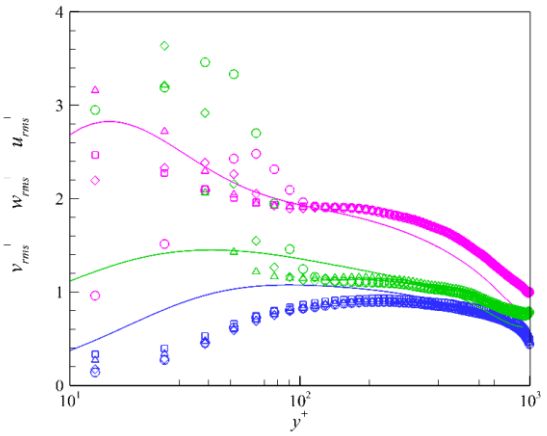

Figure 7: Vertical profiles of the turbulent intensities in turbulent open channel flow for different cases.

Figure 8 presents the three measured Reynolds shear stress components. For cases TCC1, TCC2, and TCC3, the measured Reynolds shear stresses collapse with each other very well in the region of y/h > 0.1. Meanwhile, close similarities between the measured profiles with those of the DNS results indicate that the measurement is reliable and with good accuracy. For case TCC4 where the one quarter rule is not satisfied, the profiles deviate large away from the correct profile near the free surface in figures 8(b) and 8(c). In the near wall region, the measurement errors in all Reynolds stress stresses increase with the increasing of time interval.

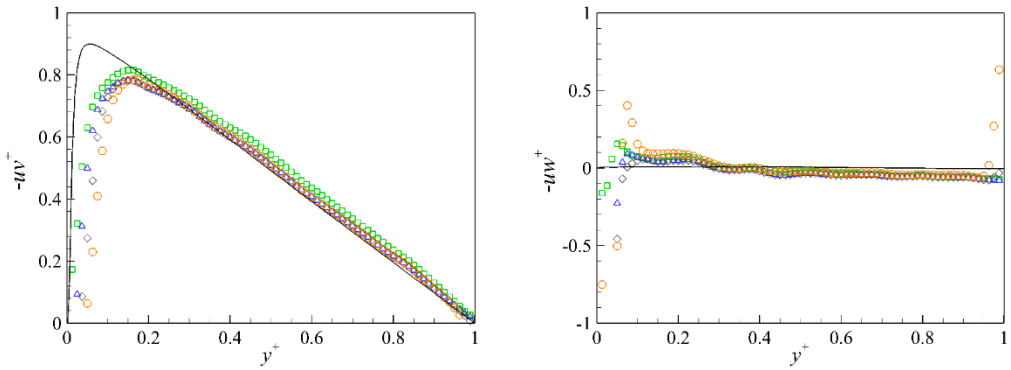

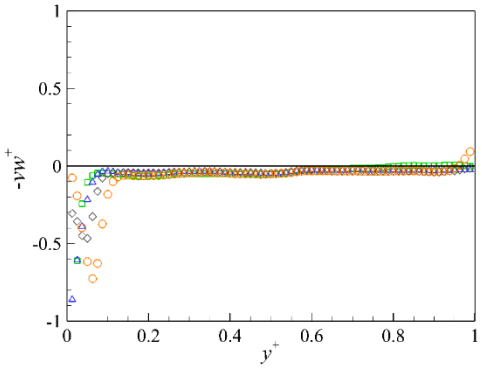

Figure 8: Vertical profiles of the Reynolds shear stresses in turbulent open channel flow for all cases.

4 Conclusions

The time interval between the two particle images in each pair is one of the crucial parameters to be optimized while performing stereo-PIV measurement. The present study investigates the influence of time interval on the measurement accuracy of stereo-PIV with a laminar flow and a turbulent open channel flow data sets.

The three-dimensional laminar flow field is characterized by two in-plane counter-rotating vortices and typical out-of-plane flows. Results with the laminar flow data set indicate that the measurement errors of stereo-PIV decreases with the increasing of time interval within the range while one-quarter rule is satisfied. However, errors in large velocity gradient regions cannot be effectively decreased by the time interval. For the turbulent open channel flow with Re_τ=1040, results indicate that the measurement accuracy in the outer region ($y^+ > 100$ or $y/h > 0.1$) is nearly independent of the time interval when the one-quarter rule is satisfied. However, the measurement error are significantly amplified in the near wall region where the velocity gradient is large.

The results indicate that the one-quarter rule should be strictly followed when performing stereo-PIV measurement. Moreover, the following two practical suggestions should be followed as well. (1) For flows with negligible velocity gradient, a larger time interval is useful for improving the measurement accuracy. (2) For flows with large velocity gradient, the spatial gradient of displacement within the interrogation window dominates the measurement accuracy, and a smaller time interval should be adopted to obtain a better measurement accuracy. A direct deduction from these two suggestions is that the near-wall region and outer-region of wall turbulence should be measurement with different stereo-PIV parameters.

Acknowledgement

This study is financially supported by the National Natural Science Foundation of China (No. 51609002). The authors are grateful to Prof. Rod La Foy for sharing the reference velocity fields of the laminar flow data set.

References

Adrian R (1997) Dynamic ranges of velocity and spatial resolution of particle image velocimetry. Measurement Science and Technology 8: 1393

Arroyo M, Greated C (1991) Stereoscopic particle image velocimetry. Measurement Science and Technology 2: 1181

Chen Q, Adrian R J, Zhong Q, Danxun L, Xingkui W (2014) Experimental study on the role of spanwise vorticity and vortex filaments in the outer region of open-channel flow. Journal of Hydraulic Research 52: 476

Ghosh S, Foysi H, Friedrich R (2010) Compressible turbulent channel and pipe flow: similarities and differences. Journal of Fluid Mechanics 648: 155

Hultmark M, Bailey S C, Smits A J (2010) Scaling of near-wall turbulence in pipe flow. Journal of Fluid Mechanics 649: 103

Kähler CJ, Astarita T, Vlachos PP, Sakakibara J, Hain R, Discetti S, La Foy R, and Cierpka C (2016) Main results of the 4th International PIV Challenge. *Experiments in Fluids* 57:97

Lawson N J, Wu J (1997a) Three-dimensional particle image velocimetry: error analysis of stereoscopic techniques. Measurement Science & Technology 8: 894

Lawson N J, Wu J (1997b) Three-dimensional particle image velocimetry: experimental error analysis of a digital angular stereoscopic system. Measurement Science & Technology 8: 1455

Prasad A, Adrian R (1993) Stereoscopic particle image velocimetry applied to liquid flows. Experiments in Fluids 15: 49

Kähler CJ, Astarita T, Vlachos PP, Sakakibara J, Hain R, Discetti S, La Foy R, and Cierpka C (2016) Main results of the 4th International PIV Challenge. *Experiments in Fluids* 57:97

Stanislas M, Okamoto K, Kähler C, Westerweel J, Scarano F (2008) Main results of the third international PIV challenge. Experiments in Fluids 45: 27

Sciacchitano A, Scarano F, Wieneke B (2012) Multi-frame pyramid correlation for time-resolved PIV. Experiments in Fluids 53: 1087

Soloff S M, Adrian R J, Liu Z-C (1997) Distortion compensation for generalized stereoscopic particle image velocimetry. Measurement Science and Technology 8: 1441

Westerweel J, Elsinga G E, Adrian R J (2013) Particle image velocimetry for complex and turbulent flows. Annual Review of Fluid Mechanics 45: 409

Wieneke B (2005) Stereo-PIV using self-calibration on particle images. Experiments in Fluids 39: 267